Tuning the magnetic properties of $NiPS_3$ through organic-cation intercalation

D. Tezze[1], J. Pereira[1], Y. Asensio[1], M. Ipatov[2], F. Calavalle[1], F. Casanova[1,3], A. M. Bittner[1,3], M. Ormaza[4], B. Martín-García[1], L. E. Hueso[1,3], M. Gobbi[1,3,5]

[1] CIC nanoGUNE BRTA, 20018 Donostia-San Sebastian, Spain

[2] SGIker Medidas Magnéticas Gipuzkoa, UPV/EHU, 20018 Donostia-San Sebastian, Spain

[3] IKERBASQUE, Basque Foundation for Science, 48013 Bilbao, Spain

[4] Departamento de Polímeros y Materiales Avanzados: Física, Química y Tecnología, Universidad del País Vasco, Paseo Manuel de Lardizabal 3, San Sebastián 20018, Spain

[5] Materials Physics Center CSIC-UPV/EHU, 20018 Donostia-San Sebastian, Spain

Supplementary information

Table of contents

ESI Section 1: Supplementary Methods

TBA^+ electrochemical intercalation into $NiPS_3$ bulk crystal

Tetrabutylammonium (TBA^+) cations are electrochemically intercalated into $NiPS_3$ bulk crystal (2-3 mg) by means of a home-made cell composed of two electrodes immersed in a 5 mL electrolyte solution, contained in a 40 mL glassy vial (**Fig. S1a**). The system is located in a N_2-filled glow box (H_20 < 0.1 ppm, O_2 < 0.1 ppm) at ambient temperature (23 °C). The electrolyte is a solution of tetrabutylammonium bromide (TBAB), in acetonitrile at a concentration of 2 mg/mL, dehydrated at 100 °C overnight (for the crystal presented in Fig. 1 of the main text). A silver plate is used as anode and the $NiPS_3$ crystal is the cathode, attached on a platinum plate with some indium dots (inset in **Fig. S1a**). The metallic electrodes are mechanically polished using sandpaper and sonicated in ethanol and isopropanol before usage. The crystal and the silver anode are immersed in the electrolyte and the cell closed to prevent the rapid evaporation of the solvent. The apparatus is connected to the external Keithley 2636 source meter that controls the process at constant current via a LabView program and measures the potential difference between the two electrodes as a function of time, generating the galvanostatic charge (GC) curve (red curve in **Fig. S1b**). The crystal considered in the main text was intercalated at 50 μA; employing different currents and concentration resulted in the stabilization of different structural phases in the crystals (see also ESI section 3).

The voltage generated during the intercalation can be used to monitor the electrochemical process until completion. Typically, during the intercalation the potential is approximately constant which we term the first plateau. As the process reaches its final steps (i.e. when the crystal is almost fully intercalated), the potential increases rapidly, reaching a second plateau value. This second plateau is found in a "control experiment" (reference), in which the same electrochemical process is carried out without the crystal connected to the cathodic platinum plate (black curve in **Fig. S1b**). In the control experiment, the potential increases rapidly to the final plateau; this value indicates the beginning of side reactions involving the reduction of the salt-solvent system (electrolyte) at the cathode. Thus, when the crystal is electrically connected, firstly it gets fully intercalated by TBA^+ cations at a lower potential value (corresponding to the first plateau); then, when the potential approaches the second plateau, the electrochemical process can be considered finished.

From the GC curve (red curve in **Fig. S1b**), one can extrapolate the amount of time required, $\Delta t_{int.}(TBA^+)$, for completing the intercalation, corresponding to the step of the second plateau (~ 3 h). This allows to get a first estimation of the stoichiometric index x (in TBA_xNiPS_3 unit formula) using the formula:

$$x = \frac{I \cdot M_r(NiPS_3) \cdot \Delta t_{int.}(TBA^+)}{m(NiPS_3) \cdot \mathcal{F}} \qquad \textbf{Eq.1}$$

Where x is the stochiometric index; $\mathrm{m(NiPS_3)}$ is the total mass of the pristine crystal [g]; $\mathcal{F}$ is the Faraday's constant (96485,34 C/mol); I is the current set for the intercalation process [A]; $\mathrm{M_r(NiPS_3)}$ is the molar mass of the $NiPS_3$ formula unit (160,08 g/mol). For example, we intercalated 2.52 mg of $NiPS_3$ at 30 μA; the process ended approximately in 3 h. From Eq. 1 we found x = 0.25.

A second independent evaluation of the stoichiometric index x can be extrapolated from gravimetric measurements (see ESI section 2). A comparison between these two values provide a self-consistent evaluation of the intercalate's average composition.

TBA^+ electrochemical intercalation into $NiPS_3$ exfoliated flakes

For the electrochemical intercalation of TBA^+ cations into $NiPS_3$ flakes (**Fig. S1c**), the setup configuration is essentially the previous one used for bulk-crystals. In this case, we use a 10 mL becher filled with 5 mL of the TBAB electrolyte (2mg /mL) in which we immerse cathode and anode. gold contacts prepatterned Si/SiO_2 substrate, with $NiPS_3$ flake stamped onto it (inset in **Fig. S1c**), acts as the cathode. One of the device's gold contacts is connected to the external circuit by means of a copper wire and an indium dot, and the device is lowered into the electrolyte, such that the flake is completely immersed. A silver plate is used as anode. A current of 2 mA is set for 5 minutes. In this case, the GC curve does not give any relevant information about the evolution of the electrochemical process, because most of potential drop is due to electrostatic charging of the substrate and electrolyte's side reactions on metallic surfaces.

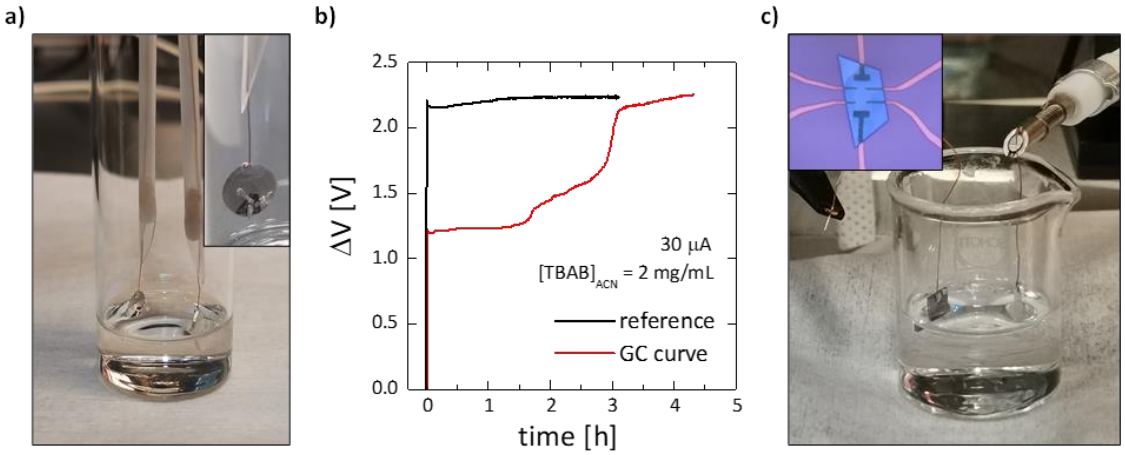

Figure S1: a) Home-made electrochemical cell setup for TBA^+ intercalation into $NiPS_3$ bulk crystal. A platinum plate (*left*) is used to hold the $NiPS_3$ crystal, electrically connected to it by means of indium pieces (*inset*) and fully immersed in the electrolyte. A silver plate (*right*) is used as anode. **b)** Galvanic charge (GC) curve of TBA^+ intercalation into $NiPS_3$ crystal (*red curve*) and the reference curve (black curve), obtained following the same process without the crystal. For the crystal shown here, Δt_{int} (TBA^+) = 3 h. **c)** Setup for the electrochemical intercalation of TBA^+ cation into exfoliated $NiPS_3$ flake stamped on gold contacts prepatterned Si/SiO_2 substrate (*inset*). The device is connected to the cathodic side while an Ag plate is used as anode.

$Co(Cp)_2^+$ intercalation via $TBA^+/Co(Cp)_2^+$ exchange into $NiPS_3$ bulk crystal & exfoliated flakes

Intercalation of $Co(Cp)_2^+$ cations into $NiPS_3$ is performed by a novel two-steps approach, exploiting a heterogeneous exchange of pre-intercalated TBA^+ cations with cobaltocenium $Co(Cp)_2^+$ in solution. Bulk TBA_xNiPS_3 crystals are immersed in a polymer vial (Eppendorf) with 1 mL of $Co(Cp)_2PF_6$ solution in acetonitrile at a concentration of 50 mg/mL (**Fig. S2**). The process is carried out in an oven located in a N_2-filled glow box (H_20 < 0.1 ppm, O_2 < 0.1 ppm) at 50 °C for 2 days. it can be carried out also at ambient temperature (23 °C) since its kinetics appear to be very fast. The higher temperature (50 °C) and longer process time are employed to completely assure the $TBA^+/Co(Cp)_2^+$ exchange for the whole crystal.

This a non-redox phenomenon which occurs spontaneously, driven by the thermodynamic. The mechanism can be generally described as:

$$TBA_xNiPS_3 + x\ Co(Cp)_2{}^+ \rightarrow\ [Co(Cp)_2]_xNiPS_3 +\ TBA^+$$

Since the pre-intercalated TBA^+ cations have a single formal charge, as also the $Co(Cp)_2^+$ cations, the pair experiences a simple 1:1 exchange.

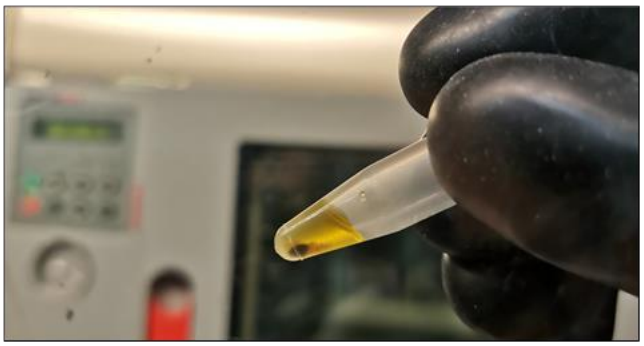

Figure S2: $TBA_{0.25}NiPS_3$ crystal dipped in a $Co(Cp)_2PF_6$ solution (50 mg/mL) during the cation exchange process that leads to the $[Co(Cp)_2]_yNiPS_3$ intercalate. After some time, a dark-red cloud is visible around the crystal, compatible with the absorption spectrum of electrochemically exfoliated $NiPS_3$[1]. This is due to a mild exfoliation of the crystal surface during the cation exchange.

ESI Section 2: Gravimetric evaluation of the stochiometric index x in TBA_xNiPS_3

The electrochemical intercalation of TBA^+ cations into $NiPS_3$ is carried out for a bulk crystal, fully immersed in the electrolyte. The process undergoes to a "self-limited" complete intercalation for the whole crystal, until VdW gaps are available to be filled with organic cations. In this way, a second independent estimation of the index x in the unit formula TBA_xNiPS_3 is accessible through mass measurements of the crystal before and after intercalation. A crystal of some milligrams is chosen as compromise between the setup limits and a sufficient accuracy of the mass variation.
For example, we selected a pristine $NiPS_3$ crystal of 2.52 mg (related to the GC curve displayed in fig. 1 of the main text); after intercalation we measured a 3.36 mg of mass with a variation Δm of 0.84 mg, equal to the total mass of the intercalated molecules. It is possible to calculate the stoichiometric index x applying the following equation (**Eq. 2**):

$$x = \frac{n(TBA^+)}{n(NiPS_3)} = \frac{\Delta m \cdot M_r(NiPS_3)}{m_p(NiPS_3) \cdot M_r(TBA^+)} \qquad \text{Eq. 2}$$

Where $\mathrm{n(TBA^+)}$ are the moles of intercalated TBA^+ cations; $\mathrm{n(NiPS_3)}$ are the moles of the unit formula of $NiPS_3$ (185.87 g/mol); $\mathrm{\Delta m}$ is the mass variation of the crystal; $\mathrm{m_p(NiPS_3)}$ is the mass of the pristine $NiPS_3$ crystal; $\mathrm{M_r(TBA^+)}$ is the relative mass of TBA^+ molecule (242.47 g/mol). We highlight that the stoichiometric index calculated through Eq. 2 is in very good agreement with that one extracted from the GC curve (see above). This validates the calculated 0.25 stoichiometric index. Moreover, we have performed the same synthesis several times, achieving x = 0.25 ± 0.02 stoichiometric index in TBA_xNiPS_3 unit formula when [TBAB] of 2 mg/mL is used. With a higher [TBAB] equal to 10 mg/mL, we found systematically x = 0.32 ± 0.01. Both intercalation processes were carried out at 30 μA. For the sample considered in the main text, we set a current of 50 μA and a [TBAB] equal to 2 mg/mL, obtaining the same 0.25 stoichiometric index.
Additionally, we elucidated by XRD analysis (see ESI section 3), that different stoichiometries of TBA_xNiPS_3 intercalate correspond to different crystallographic phases.

ESI Section 3: X-ray diffraction

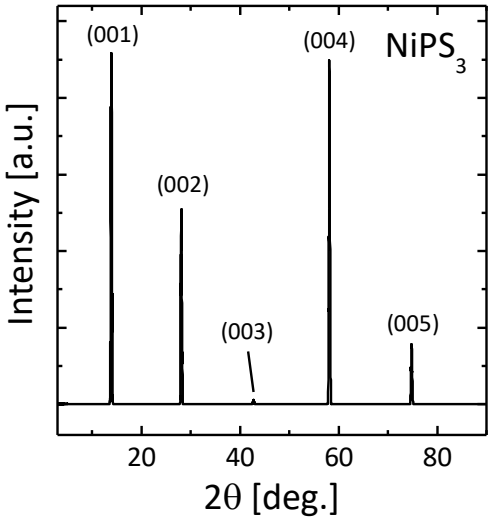

Figure S3: X-ray diffractograms of pristine $NiPS_3$ bulk crystal in the 3 deg. - 80 deg. range in 2θ.

$NiPS_3$		
(00l)	**2θ [deg.]**	**FWHM[deg.]**
(001)	13.9(3)	0.2(4)
(002)	28.1(0)	0.2(3)
(003)	42.7(5)	0.2(3)
(004)	58.1(5)	0.2(3)
(005)	74.8(2)	0.2(5)

Table S1: 2θ values and the full width at half maximum (FWHM) of the (00l) peaks of pristine $NiPS_3$. Due to the high crystallinity of pristine $NiPS_3$, the interlayer distance can be calculated very precisely through the Bragg's law ($2d \sin(\theta)=n\lambda$). We extracted the following value, in agreement with values reported in literature[2]:

$$d(NiPS_3) = (6.34 \pm 0.01)\ \text{Å}$$

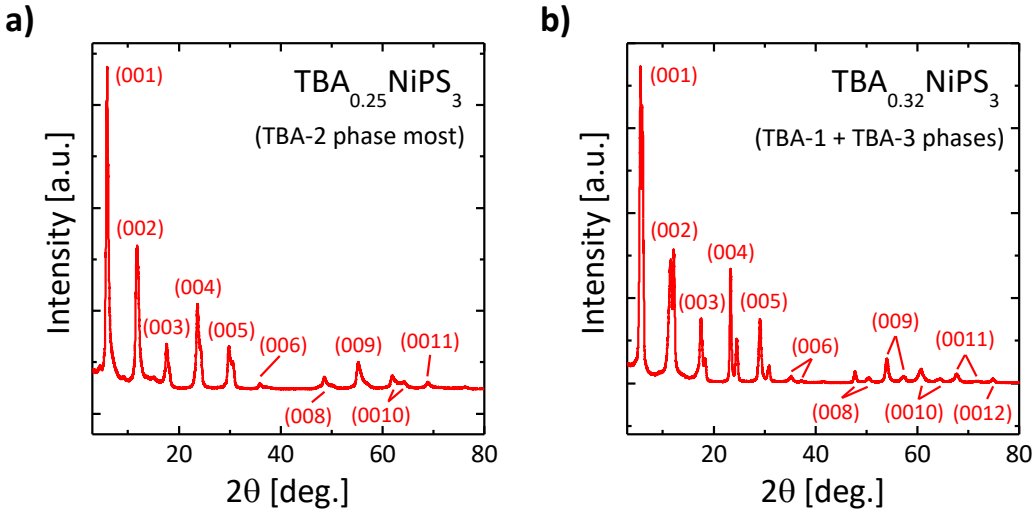

Figure S4: (a) XRD pattern for the $TBA_{0.25}NiPS_3$ intercalated at 50 µA using [TBAB] = 2 mg/mL (sample reported the main text). **(b)** full-range (3-80 deg. in 2θ) XRD pattern for the $TBA_{0.32}NiPS_3$ intercalated at 30 µA using [TBAB] = 10 mg/mL. We found a stoichiometric index x = 0.25 for the sample in **(a)**, composed mostly by TBA-2 phase and x = 0.32 for the bi-phasic sample in **(b)** (TBA-1 and TBA-3). Each of the phases are well characterised by different interlayer distances. Three families of (00l) peaks could be distinguished (see also table S2), which can be assigned to three structural phases. The sample shown in **(a)**, which is the sample considered in the main text, is characterized by a predominant phase, called TBA-2 in Table S2. The peaks corresponding to phase TBA-1 and TBA-3 are also detectable, albeit with lower intensity. Conversely, in the sample in **(b)**, we clearly distinguish a mixture of the phases TBA-1 and TBA-3, and the peaks associated to the two phases present a similar intensity.

TBA_xNiPS_3						
(00l)	Phase TBA-1		Phase TBA-2		Phase TBA-3	
	2θ [deg.]	**FWHM[deg.**	**2θ [deg.]**	**FWHM[deg.**	**2θ [deg.]**	**FWHM[deg.**
(001)	5.(6)	0.(4)	5.(8)	0.(2)	6.(1)	0.(3)
(002)	11.4(7)	0.(7)	11.8(2)	0.(4)	12.1(6)	0.3(6)
(003)	17.51	0.5(2)	17.6(6)	0.5(3)	18.3(1)	0.3(4)
(004)	23.3(2)	0.3(2)	23.6(6)	0.4(0)	24.5(2)	0.4(2)
(005)	29.11	0.4(9)	30.5(6)	0.5(8)	30.8(2)	0.5(0)

Table S2: 2θ values and the full width at half maximum (FWHM) of the (00l) peaks of $TBA_{0.25}NiPS_3$. Three families of peaks were found by performing the electrochemical intercalation using different parameters (in particular, the intercalation current and TBAB concentration). The three families of peaks correspond to slightly different interlayer distances:

$$d(TBA1) = (15.3 \pm 0.1)\ \text{Å} \qquad d(TBA2) = (15.0 \pm 0.1)\ \text{Å} \qquad d(TBA3) = (14.5 \pm 0.1)\ \text{Å}$$

We assign the different phases to different orientation of the TBA^+ cations between the $NiPS_3$ layers.

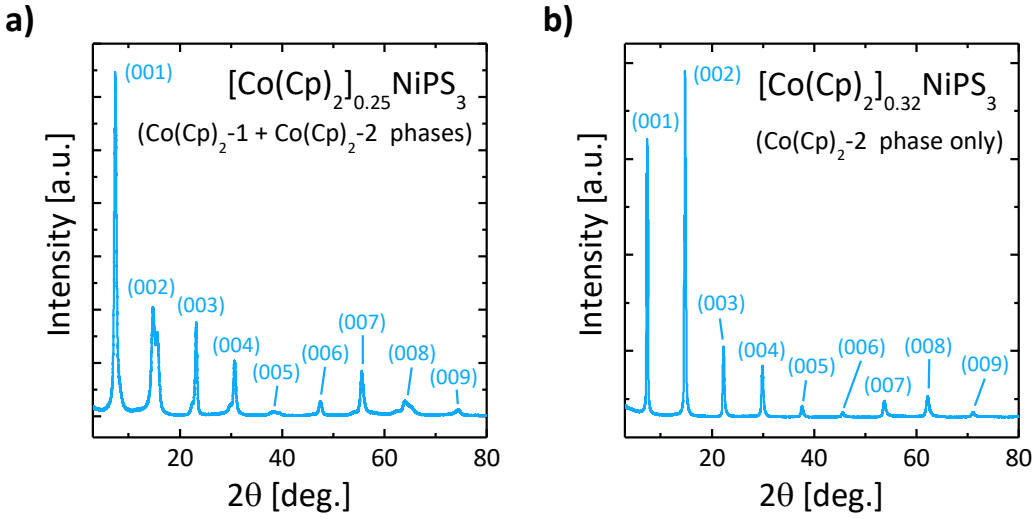

Figure S5: (a,b) full-range (3-80 deg. in 2θ) XRD pattern for $Co(Cp)_2^+$ intercalated $NiPS_3$ crystals, derived by the ion exchange of two different TBA^+ intercalated $NiPS_3$ crystals: **(a)** $TBA_{0.25}NiPS_3$ obtained at 50 µA with [TBAB] of 2 mg/ml and **(b)** $TBA_{0.32}NiPS_3$, obtained at 30 µA with [TBAB] of 10 mg/ml. The sample in **(a)**, $[Co(Cp)_2]_{0.25}NiPS_3$, which is the sample also considered in the main text, is characterized by two families of peaks with comparable intensity, which correspond to two structural crystalline phases (see also table S2). Conversely, the sample in **(b)**, $[Co(Cp)_2]_{0.32}NiPS_3$, displays only one phase (called 1 in Table S3).

$[Co(Cp)_2]_xNiPS_3$				
(00l)	Phase $Co(Cp)_2$-1		Phase $Co(Cp)_2$-2	
	2θ [deg.]	**FWHM[deg.]**	**2θ [deg.]**	**FWHM[deg.]**
(001)	7.(4)	0.3(1)	7.(5)	0.3(2)
(002)	14.(8)	0.5(1)	15.(5)	0.5(9)
(003)	22.(4)	0.5(4)	23.(1)	0.4(0)
(004)	29.(9)	0.6(8)	30.(7)	0.4(1)
(005)	-	-	-	-
(006)	46.(1)	1.(2)	47.(4)	0.(6)

Table S3: 2θ values and the full width at half maximum (FWHM) of the (00l) peaks of $[Co(Cp)_2]_{0.25}NiPS_3$ and $[Co(Cp)_2]_{0.32}NiPS_3$. Two families of peaks were found by performing the ion exchange process on $TBA_{0.25}NiPS_3$. The two families of peaks correspond to slightly different interlayer distances:

$$(Co(Cp)_2 1) = (11.9 \pm 0.1)\ \text{Å} \quad (Co(Cp)_2 2) = (11.5 \pm 0.1)\ \text{Å}$$

We ascribe the different phases to different orientation of the $Co(Cp)_2^+$ cations between the $NiPS_3$ layers. In particular, we assign phase $Co(Cp)_2$-1 to a structural phase in which $Co(Cp)_2^+$ cations are oriented vertically between the layers (see main text), whereas $Co(Cp)_2$-2 to another one in which $Co(Cp)_2^+$ cations are oriented horizontally between the layers. As discussed in the main text, it could be that $Co(Cp)_2$-1 presents a more complex assembly of vertically and horizontally oriented molecules.

ESI Section 4: Raman spectroscopy

Bulk $NiPS_3$ has a monoclinic unit cell (space group C 2/m) with the point group C_{2h}. However, if the interlayer coupling is treated as a small correction, phonon modes can instead be labelled in terms of the D_{3d} point group of the hexagonal $NiPS_3$ monolayer. For spectra acquired in a backscattering geometry, the zone center phonon modes (first-order processes) are represented by the irreducible representation, $\Gamma = 3A_{1g} + 2A_{2g} + A_{1u} + 4A_{2u} + 5E_g + 5E_u$, that predicts 8 Raman-active ("even-symmetry") phonon modes ($3A_{1g} + 5E_g$), all of them experimentally well observed for bulk pristine $NiPS_3$ in resonant conditions[3]. We decided to use a 633 nm laser to fit this condition and explore the Raman spectrum's evolution upon TBA^+ electrochemical intercalation and subsequent $TBA^+/Co(Cp)_2^+$ exchange.

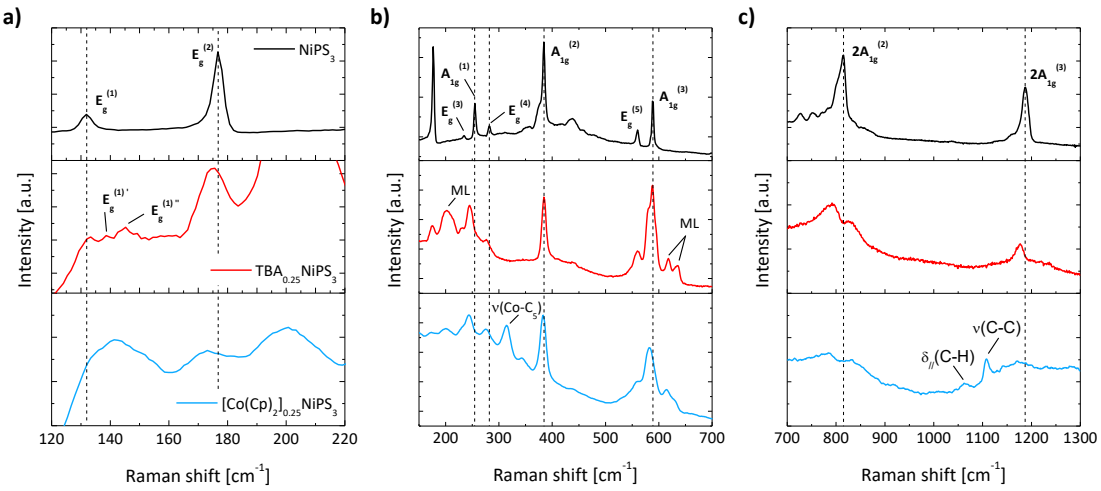

Figure S6: (a-c) Raman spectra of bulk crystals of pristine $NiPS_3$ (black curve), $TBA_{0.25}NiPS_3$ (red curve) and $[Co(Cp)_2]_{0.25}NiPS_3$ (blue curve). The spectra are reported in different ranges for clarity: (**a**) 120-220 cm^{-1}, (**b**) 150-700 cm^{-1} and (**c**) 700-1300 cm^{-1}. Spectra have been taken on a fresh-cleaved internal crystal's surface, to avoid possible contamination by TBAB or $Co(Cp)_2PF_6$ salts on the external surfaces.

As highlighted in the main text, the $E_g^{(1)}$ peak at 132 cm^{-1} is strongly suppressed in intensity after intercalation (**Fig. S6a**). This mode is related to the collective translational mode of Ni(II) cations in their sulphur coordinated octahedral sites (Oh sites)[4]. Here, we note that the $E_g^{(1)}$ peak is also slightly blue-shifted from the pristine one to 133 cm^{-1} and more broadened. These features are compatible with a decrease of the density of Ni(II) located at the pristine Oh sites and to a vacancies-induced distortion of the coordination geometry as a result. Ni(II) cations are reported to be the reduction "hotspots" of the electrochemical process. In this way, Ni^0 metallic atoms are formed. Moreover, an intralayer displacement from their octahedral site to an adjacent sulphur-coordinated tetrahedral (Td sites) site was proposed basing on ^{31}P NMR[5], EXAFS[6], XPS[7] studies, supported by XRD and Magnetization measurements[8] for Li^+ intercalated $NiPS_3$.

In $TBA_{0.25}NiPS_3$, two new distinguishable low-frequency Raman peaks (labelled $E_g^{(1)}$ ' and $E_g^{(1)}$ '') appear at 138.5 cm^{-1} and 145.5 cm^{-1} (**Fig. S6a**). These were ascribed to a translational symmetry-breaking effect on the Raman signal in the few layers and monolayer $NiPS_3$ limit[3]. Additionally, as mentioned in the main text, new broad peak at 202 cm^{-1} and two others well resolved peaks

(labelled with ML in **Fig. S6b**) appear in $TBA_{0.25}NiPS_3$ Raman spectra at 618 cm^{-1} and 635 cm^{-1}, which are signature of translational symmetry breaking, and can also be observed in atomically thin layers.

At higher frequencies, peaks are mostly associated to the intramolecular vibrations from the $(P_2S_6)^{4-}$ bipyramidal structures. We observed red shifts, splitting or unchanging of peaks' positions upon TBA^+ electrochemical intercalation. In details, $E_g^{(2)}$ (176.5 cm^{-1}), $E_g^{(3)}$ (234.5 cm^{-1}), $A_{1g}^{(1)}$ (254.5 cm^{-1}) and the $E_g^{(4)}$ (282 cm^{-1}) move to 175 cm^{-1}, 230.5 cm^{-1}, 245 cm^{-1} and 277 cm^{-1}, respectively (**Fig. S6b**). Interestingly, the evolution of the $A_{1g}^{(1)}$ peak's position follows the same trend found for the Li^+ intercalated $NiPS_3$[9]. The shift magnitude is remarkably high but less pronounced than in the Li case, probably due to the relative lower intercalated ions per unit formula (0.25) because of the limiting vdW molecular hindrance of TBA^+ respect Li^+ ions. The $A_{1g}^{(2)}$, $E_g^{(5)}$ and $A_{1g}^{(3)}$ peaks at 384.5 cm^{-1}, 560 cm^{-1} and 588.5 cm^{-1} are unaltered in position in the $TBA_{0.25}NiPS_3$, but broader than the pristine ones (**Fig. S6b**). For $[Co(Cp)_2]_{0.25}NiPS_3$, these features experience a weak red-shift to 383 cm^{-1}, 558 cm^{-1} and 582 cm^{-1}.

Finally, we observed a splitting of both the complex second-order Raman pristine peaks, the $2A_{1g}^{(2)}$ (814.5 cm^{-1}) and the $2A_{1g}^{(3)}$ (1187 cm^{-1}) into two broader convoluted peaks at lower and higher Raman shift, located around 790 cm^{-1} and 825 cm^{-1} for the former and at 1176 cm^{-1} and 1223 cm^{-1} for the latter (**Fig. S6c**). This can be seen also as a prominent red-shift of the pristine peaks and the appearance of a new peak due to a symmetry breaking effect at the few-layer limit, as mentioned before for the other previous Raman peaks. In the $[Co(Cp)_2]_{0.25}NiPS_3$ intercalate, they appear much more broadened. In general, broadening of the peaks can be related intrinsically to the characteristics of the monolayer or to crystal lattice deformations induced by the electrochemical intercalation of TBA^+ and their exchange with $Co(Cp)_2^+$.

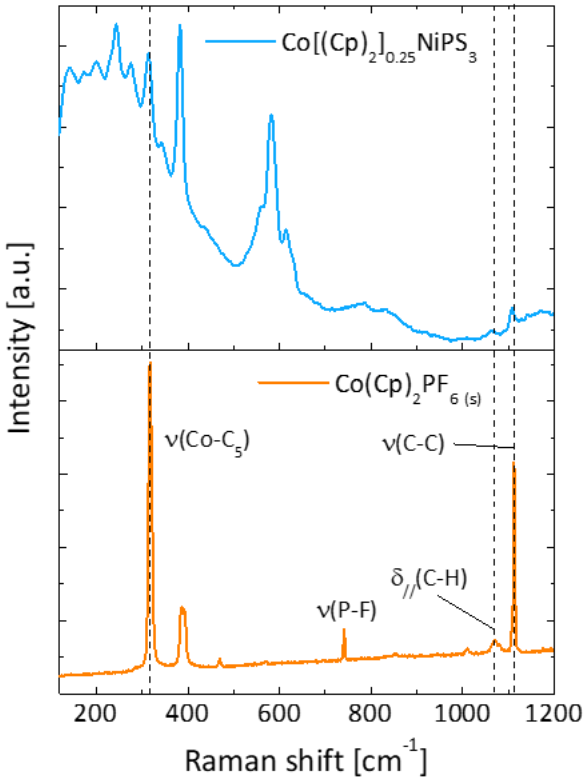

Figure S7: Raman spectra of $Co[(Cp)_2]_{0.25}NiPS_3$ (*blue curve*) and $Co(Cp)_2PF_6$ salt (*orange curve*). In $Co[(Cp)_2]_{0.25}NiPS_3$, the most intense Raman peaks of $Co[(Cp)_2]^+$ are observed at 314 cm^{-1} $\nu(Co - C_5)$, 1062 cm^{-1} $\delta_{//}(C - H)$ and 1108 cm^{-1} $\nu(C - C)$, interestingly red-shifted respect the pristine Cobaltocenium's peaks, located at 317 cm^{-1}, 1070 cm^{-1} and 1112.5 cm^{-1}. Conversely, the counter anion's (PF_6^-) main Raman peak at 741 cm^{-1} $\nu(P - F)$ is not detected even if its relative maximum intensity in $Co(Cp)_2PF_6$ Raman spectrum is more the double respect the one at 1070 cm^{-1}. Both of the observation prove the real intercalation of the cationic specie.

ESI Section 5: Magnetic properties of intercalates

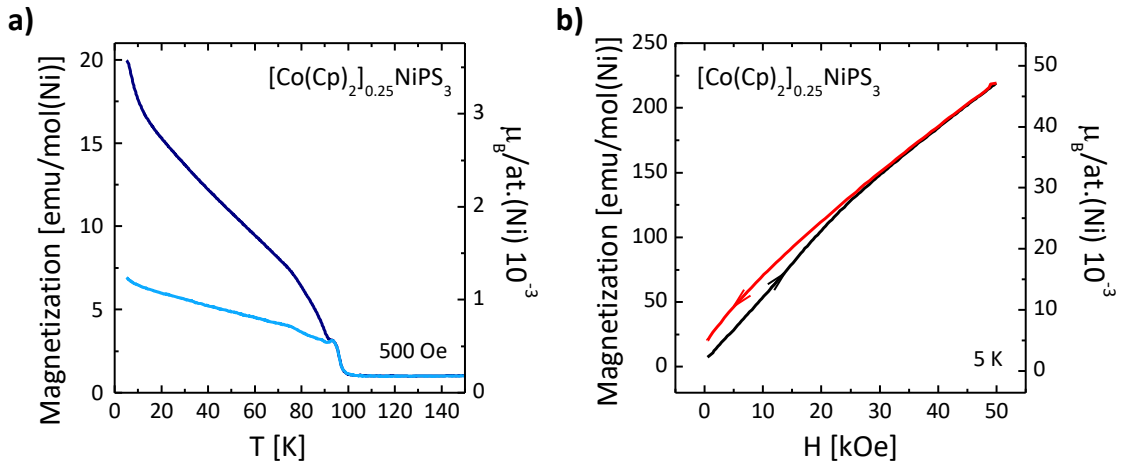

Figure S8: (a) Light blue: Field-cooled $[Co(Cp)_2]_{0.25}NiPS_3$ magnetization curve M(T). An external field H = 500 Oe was applied during the cooling process and during the measurement of the M(T) from low to high temperature. Dark blue: Temperature dependence of the magnetization measured with H = 500 Oe after applying 5 T at 5K. **(b)** A minor loop measured at 5K for the same crystal field cooled at 500 Oe shows how the application of 5T drives the system in a different magnetic state, characterized by a larger remanence. These data indicate that the magnetic state of $[Co(Cp)_2]_{0.25}NiPS_3$ is rather complex. In particular, there is a magnetic moment in the system which is not saturated by the external field (500 Oe) applied during the cooling process. This indicates that there might be magnetic interactions which persist up to high temperatures, albeit involving only a few uncompensated Ni atoms.

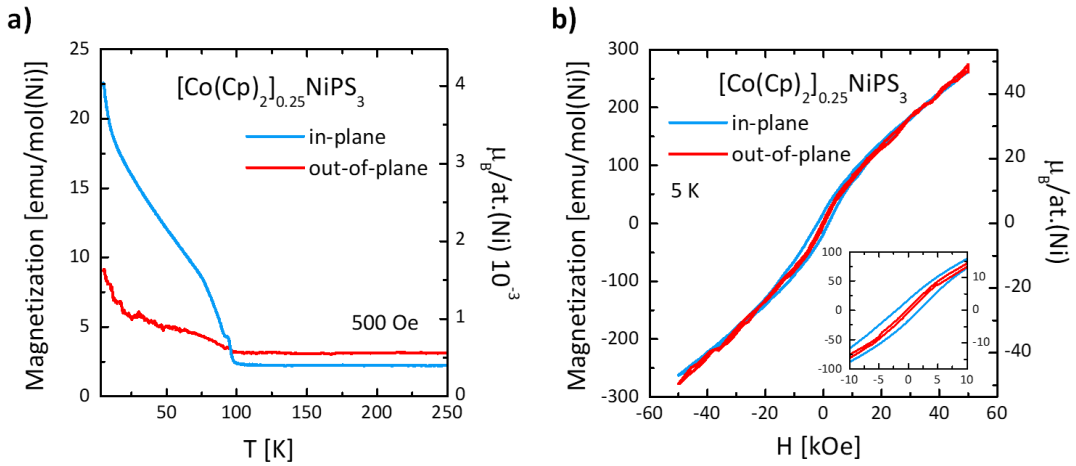

Figure S9: (a) Field cooled magnetization M(T) and (b) hysteresis M(H) measured for a $[Co(Cp)_2]_{0.25}NiPS_3$ crystal with the field applied in plane and out of plane. The hysteresis measured with the magnetic field applied in the plane displays larger coercive fields. This indicates that the crystal possesses a magnetic anisotropy displaying an in-plane magnetic easy axis. We highlight that the pristine $NiPS_3$ crystals possess an XY antiferromagnetism, in which the spins are oriented in the plane. Moreover, we highlight that these curves were recorded for the same sample shown in the main text (Fig. 4a), 45 days after the measurement displayed in the main text. The crystal was stored in air. Only minor changes were observed in the hysteresis loop indicating a remarkable air stability of the crystal.

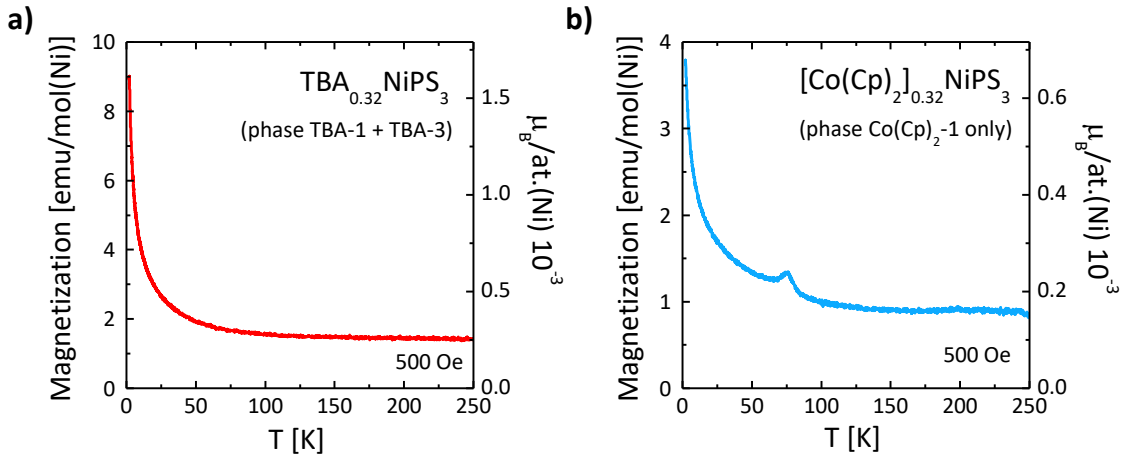

Figure S10: Field cooled magnetization M(T) recorded for (a) $TBA_{0.32}NiPS_3$ (obtained at 30 μA and [TBAB] = 10 mg/mL) and (b) $[Co(Cp)_2]_{0.32}NiPS_3$ (obtained from the previous one by cation exchange). The XRD patterns of $TBA_{0.32}NiPS_3$ is shown in Fig. S4b; it is characterized by the phases TBA1 and TBA3 in Table S2. The XRD patterns of $[Co(Cp)_2]_{0.32}NiPS_3$ is shown in Fig. S5b; it displays only the phases $Co(Cp)_2$-1 in Table S3. Since the M(T) do not show a clear ferrimagnetic phase transition, we conclude that the ferrimagnetic signals presented in the main text originate from phase TBA-2 for TBA^+ intercalated $NiPS_3$ and phase $Co(Cp)_2$-1 for $Co(Cp)_2^+$ intercalated $NiPS_3$.

References

1 X. Li, Y. Fang, J. Wang, B. Wei, K. Qi, H. Y. Hoh, Q. Hao, T. Sun, Z. Wang, Z. Yin, Y. Zhang, J. Lu, Q. Bao and C. Su, *Small*, 2019, **15**, 1902427.

2 B. E. Taylor, J. Steger and A. Wold, *Journal of Solid State Chemistry*, 1973, **7**, 461–467.

3 C.-T. Kuo, M. Neumann, K. Balamurugan, H. J. Park, S. Kang, H. W. Shiu, J. H. Kang, B. H. Hong, M. Han, T. W. Noh and J.-G. Park, *Sci Rep*, 2016, **6**, 20904.

4 M. Bernasconi, G. L. Marra, G. Benedek, L. Miglio, M. Jouanne, C. Julien, M. Scagliotti and M. Balkanski, *Phys. Rev. B*, 1988, **38**, 12089–12099.

5 C. Berthier, Y. Chabre and M. Minier, *Solid State Communications*, 1978, **28**, 327–332.

6 G. Ouvrard, E. Prouzet, R. Brec and H. Dexpert, *Journal of Solid State Chemistry*, 1991, **91**, 271–278.

7 G. M. Currò, V. Grasso, F. Neri and L. Silipigni, *Il Nuovo Cimento D*, 1995, **17**, 37–52.

8 R. Brec, *Solid State Ionics*, 1986, **22**, 3–30.

9 I. Kerrache, C. Julien and C. Sourisseau, *Solid State Ionics*, 1996, **92**, 37–43.